

Short Communication

## Corrosion Inhibition Effect of flubendazole for Carbon Steel in 0.5 M H<sub>2</sub>SO<sub>4</sub>

Wei Chen<sup>1</sup>, Wenwen Xiao<sup>1,2,\*</sup>

<sup>1</sup> SINOPEC Northwest Company of China Petroleum and Chemical Corporation, Urumqi 830011, China

<sup>2</sup> Key Laboratory of Enhanced Oil Recovery in Carbonate Fractured-vuggy Reservoirs, SINOPEC, Urumqi 830011, China

\*E-mail: [xiaoww.xbsj@sinopec.com](mailto:xiaoww.xbsj@sinopec.com)

Received: 3 December 2021 / Accepted: 29 January 2022 / Published: 4 March 2022

---

The corrosion inhibition performance of flubendazole toward the corrosion of carbon steel (CS) in 0.5 M H<sub>2</sub>SO<sub>4</sub> was studied. Flubendazole adsorb on CS surface mainly through benzene ring, hydroxyl group and aromatic ring attached to benzene ring, the adsorption of flubendazole on CS surface follows Langmuir isotherm. Electrochemical results show the corrosion inhibition efficiency values of flubendazole increases with the increasing of the inhibitor concentration, and the maximum inhibition efficiency value is 93%.

---

**Keywords:** Corrosion Inhibition; Mild steel; Acid corrosion; Adsorption

### 1. INTRODUCTION

The corrosion reaction process of metals in nature is constantly occurring. Every year, the economic loss caused by corrosion is huge all over the world [1-4]. In addition, corrosion also brings a lot of inconvenience to people's life. Many organic compounds have good adsorption performance through their own structure containing functional groups, unsaturated bond structure and aromatic rings [5-10]. This spontaneous adsorption behavior can create a protective film on the metal surface, drag the migration path of corrosive particles, and slow down the corrosion reaction process of the metals [2, 11-14].

The electronegativity of heteroatoms (nitrogen, oxygen, sulfur, phosphorus) are strong, that is, the ability of these atoms in attracting electrons in compounds is relatively excellent. The metal surface can be protected well due to the adsorption bonding and feedback bonding process between these heteroatoms and metal surface [15-21]. Several unsaturated bonds such as double bond structure,  $\pi$ -bond

structure, unsaturated functional groups and etc., are potential inhibitors which can adsorb on metal surface mainly through absorb electrons from metal [22, 23].

Flubendazole (FBD) molecule has several unsaturated functional groups, atomic rings and heteroatoms in its structure, the molecular structure has potential adsorption ability and can be used as corrosion inhibitor for metals. Therefore, FBD was used as the corrosion inhibitor for carbon steel in 0.5 M H<sub>2</sub>SO<sub>4</sub>, the corrosion protection performance was studied.

## 2. EXPERIMENTAL

### 2.1 Materials preparation

Carbon steel (CS), mass fraction of element is C, 0.200%; Si, 0.350% , Mn, 1.400%; P, 0.020%; S, 0.015% was used as the working electrode during the electrochemical test process, the working electrode was encapsulated in epoxy resin and have an exposed area of 1 cm<sup>2</sup>. Before we run the lab tests, the working electrode surface is deoiled by anhydrous ethanol and polished by metallographic sandpaper to obtain a bright metal surface, then the surface was cleaned with deionized water, anhydrous ethanol and blow dry with a hair dryer. The flubendazole (CAS No. 15217-53-5, FBD, shown in Fig. 1) was bought from Shanghai Yuanye Biotechnology Co., LTD, the purity of the FBD is 99.5% and was used as received.

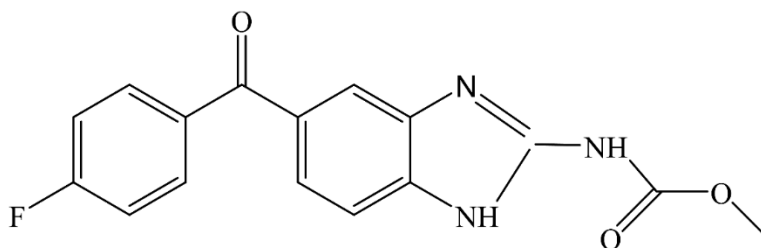


**Figure 1.** Chemical structure of FBD

### 2.2 Electrochemical tests and Surface morphology observation

Electrochemical tests were performed in a three-port flask. During the test, CS steel was used as the working electrode, the reference electrode was saturated calomel electrode while Platinum plate serve as auxiliary electrode (the purity of the platinum sheet is 99.99% and the area of the electrode is 3 cm<sup>2</sup>). The total duration of the open circuit potential test is 30 minutes, so that the electrochemical test system is in equilibrium. Ac electrochemical impedance tests were performed at open circuit potential, the sine wave was 5 mV. The potentiodynamic polarization curve was recorded at the potential range from -0.75 mV Vs. SCE to -0.25 mV Vs. SCE and the scan rate was 1 mV s<sup>-1</sup>. The morphology of the corroded surfaces was observed using Zeiss scanning electron microscope (ZEISS Scanning Mirror Co.).

### 2.3 Calculation details

The flubendazole molecule was created using Materials Studio software. The structure was optimized using Dmol<sup>3</sup> module. The relative parameters were as follows, the accuracy of simulation calculation is fine, and GGA/PBE functional was used, under the basis set DND and the basis file is 3.5, the structure of the molecule was optimized and its related properties were calculated, including the lowest unoccupied molecular orbital (LUMO), highest occupied molecular orbital (HOMO) and the dipole moment of the flubendazole was calculated.

## 3. RESULTS

### 3.1 Open circuit potential and polarization curves

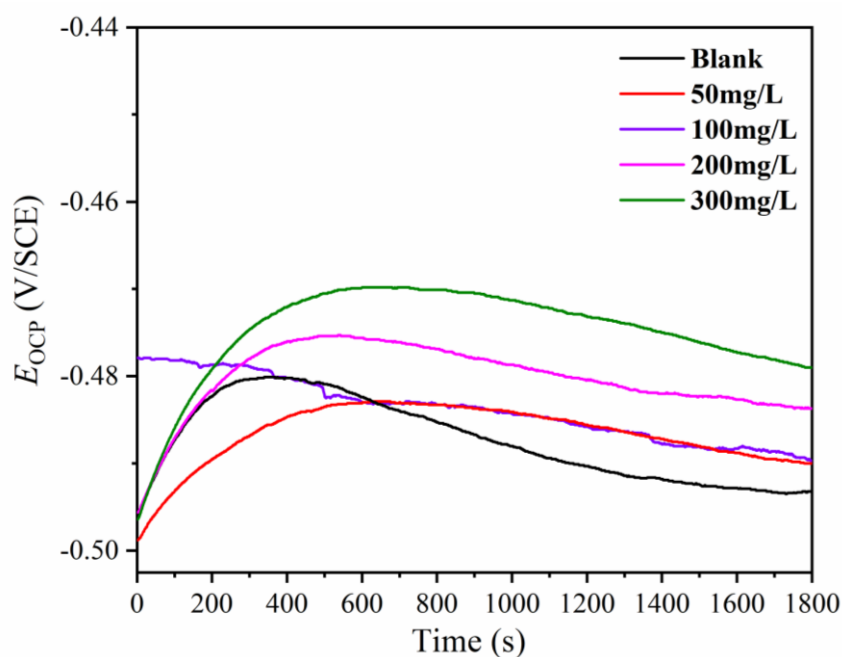


**Figure 2.** Open circuit potential of CS in 0.5 M H<sub>2</sub>SO<sub>4</sub> without inhibitor and with different concentrations of flubendazole

Corrosion potential and corrosive current density can be used to describe the corrosion tendency of metal materials in a specific corrosive environment and the intensity of the actual corrosion reaction process. In order to give a better understanding of this, the open circuit potential and potentiodynamic polarization curves of CS in 0.5 M H<sub>2</sub>SO<sub>4</sub> without inhibitor and with different concentrations of flubendazole were displayed. As shown in Figure 2, the potential increase first and then tend to be gentle, the steady state of each sample last until the end of the test. Curves for steel under 50mg /L FBD and 100mg /L FBD showed almost no significant difference in open circuit potential, while the corrosion potential of the CS under the 100mg /L FBD addition environment moved to the more positive position.

As shown in Figure 3, with the increasing of corrosion inhibitor concentration, the anodic and cathodic polarization curves move downward. In comparison to the anodic curve of the sample in the

uninhibited, transition platform area appears in the anodic curve of the samples in the inhibited 0.5 M H<sub>2</sub>SO<sub>4</sub> solution containing flubendazole, the phenomenon dues to the adsorption of inhibitor molecules on the metal surface.

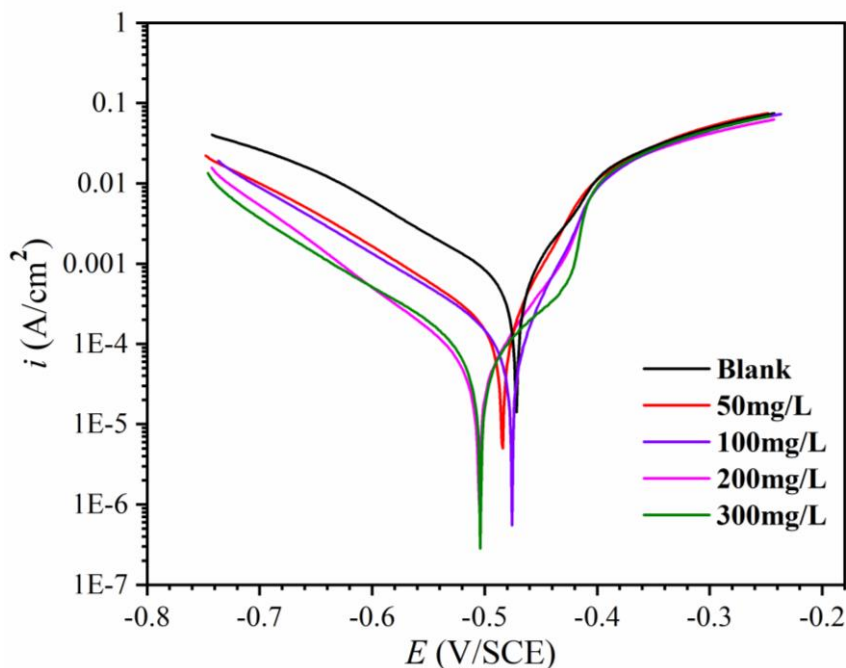


**Figure 3.** Potentiodynamic polarization curves of CS in 0.5 M H<sub>2</sub>SO<sub>4</sub> without inhibitor and with different concentrations of flubendazole

The fitted parameters for potentiodynamic polarization curves under various conditions were displayed in Table 1, the corrosion potential ( $E_{corr}$ ) value for steel in the uninhibited solution is  $-471.6$  mV Vs. SCE, all corrosion potential of these samples moves to the more positive position with the increasing of the inhibitor concentration, and the different between these corrosion potential is less than 85 mV, flubendazole worked as mixed type of inhibitor for CS in 0.5 M H<sub>2</sub>SO<sub>4</sub> with mainly control of the anodic process [24-26].

Corrosion inhibition efficiency ( $\eta$ ) is an important aspect to evaluate the corrosion protection ability of the inhibitor. The  $\eta$  values of samples in conditions with various concentrations of inhibitors were calculated according to the formula as follow:

$$\eta\% = \frac{i^0 - i}{i^0} \times 100\% \quad (1)$$

where  $i^0$  is the corrosion current density of CS steel in the corrosion condition without inhibitor,  $i$  is the corrosion current density of CS steel in the corrosion condition with inhibitor.

The calculated  $\eta$  values increases with the increasing of the flubendazole concentration, while the corrosion current density values decrease. Flubendazole shows good inhibition performance toward the corrosion of CS steel in 0.5 M H<sub>2</sub>SO<sub>4</sub>.

**Table 1.** Potentiodynamic polarization curve parameters for CS in 0.5 M H<sub>2</sub>SO<sub>4</sub> without inhibitor and with different concentrations of flubendazole

C (mg/L)	$E_{corr}$ (mV/SCE)	$i_{corr}$ ( $\mu\text{A cm}^{-2}$ )	$\beta_a$ (mV dec <sup>-1</sup> )	$\beta_c$ (mV dec <sup>-1</sup> )	$\eta$ (%)
0	-472	491.2	56	-99	-
50	-484	124.1	40	-81	74.74
100	-475	63.1	35	-58	87.15
200	-504	45.5	70	-66	90.73
300	-505	34.4	48	-68	93.00

3.2 EIS analysis

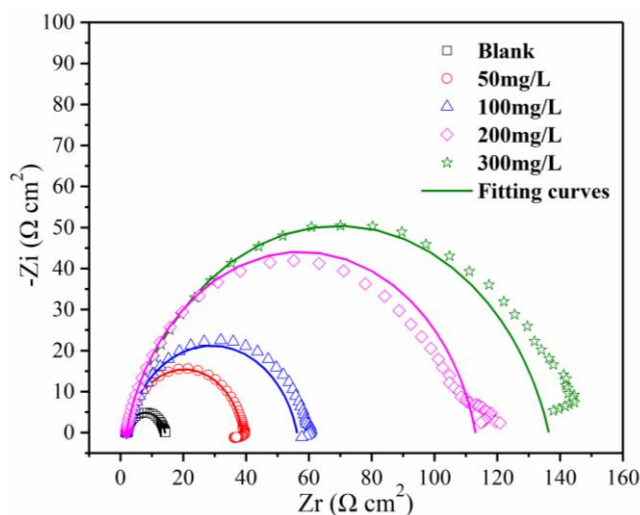


**Figure 4.** Nyquist plots of CS in 0.5 M H<sub>2</sub>SO<sub>4</sub> without inhibitor and with different concentrations of flubendazole

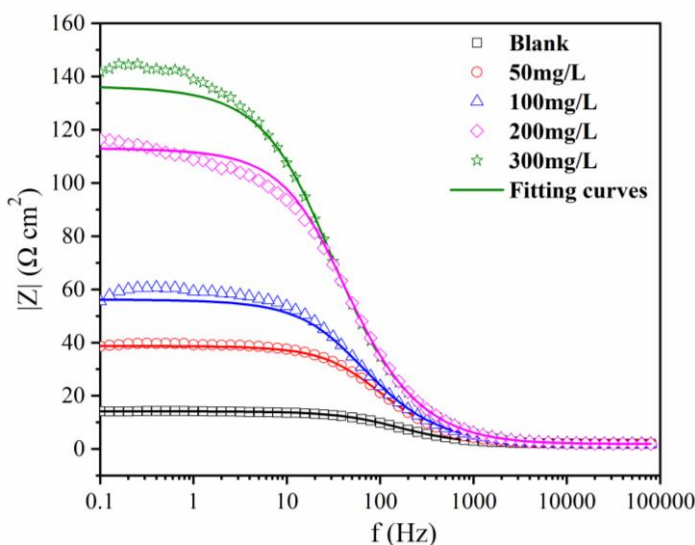


**Figure 5.** Bode plots of CS in 0.5 M H<sub>2</sub>SO<sub>4</sub> without inhibitor and with different concentrations of flubendazole

**Table 2.** Nyquist curve parameters for CS in 0.5 M H<sub>2</sub>SO<sub>4</sub> without inhibitor and with different concentrations of flubendazole

<i>C</i> (mg/L)	<i>R<sub>s</sub></i> (Ω cm <sup>2</sup> )	<i>R<sub>ct</sub></i> (Ω cm <sup>2</sup> )	<i>CPE</i> (10 <sup>-4</sup> Ω <sup>-1</sup> s <sup><i>n</i></sup> cm <sup>-2</sup> )	<i>n</i>	<i>η</i> (%)
0	1.9	12.25	3.04	0.85	
50	1.9	48.45	1.20	0.87	74.71
100	1.9	74.29	1.54	0.84	83.51
200	1.9	111.2	1.05	0.85	88.98
300	2.2	134.1	1.37	0.82	90.86

The Nyquist plots of CS in 0.5 M H<sub>2</sub>SO<sub>4</sub> without inhibitor and with different concentrations of flubendazole were shown in Fig. 4, diameter of the circuit can be used to describe the corrosion tendency of the steel. The diameter of the steel in the flubendazole containing condition is larger than that of the sample in the uninhibited condition, while the diameter of the Nyquist plots increases with the increasing of the inhibitor concentration. All Nyquist plots exhibit inductive arc resistance characteristic, accordingly, all Nyquist plots were fitted using R(QR) model [22, 27, 28]. Relative parameters obtained from the fitting of the Nyquist curve were listed in Table 2, charge transfer resistance (*R<sub>ct</sub>*) of the CS steel increasing with the increasing of the flubendazole concentration, the corrosion inhibition efficiency values were calculated according to the formula as follow:

$$\eta\% = \frac{R^0 - R}{R^0} \times 100\% \quad (2)$$

where the *R* is the charge-transfer resistance of CS steel in the uninhibited condition, *R<sup>0</sup>* is the charge-transfer resistance of CS steel in the inhibited condition. The *R<sub>ct</sub>* values and the *η* values increase with the increasing of the flubendazole concentration, which shows the same tendency with the corrosion inhibition efficiency values obtained according to the corrosion current density values.

### 3.3 Adsorption analysis

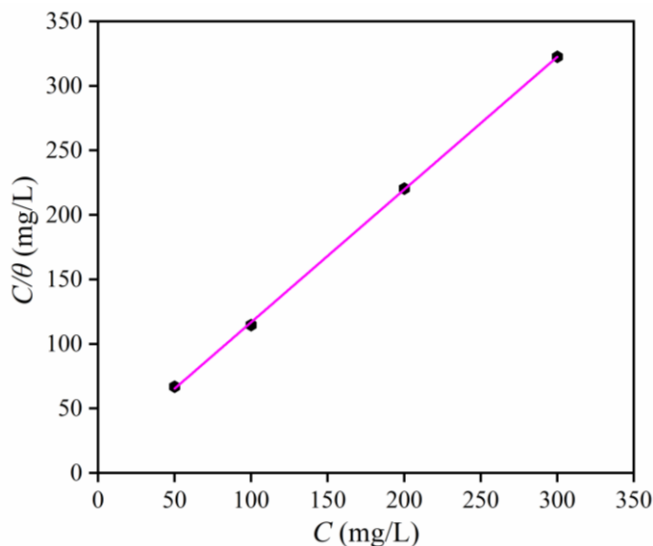


**Figure 6.** Langmuir adsorption isotherm for flubendazole at room temperature

Adsorption isotherm is a mathematical formula expressing the relationship between adsorption capacity and solution concentration under the condition of fixed temperature. As shown in Fig. 6, the relationship between  $C$  and  $C/\theta$  conforms to Langmuir adsorption isothermal adsorption law, indicating single layer of flubendazole formed on CS surface, and the inhibitor adsorb on CS surface uniformly. The equilibrium constant is 71.23 and the Gibbs free energy is  $-27.68 \text{ kJ mol}^{-1}$ , indicating the adsorption of the corrosion inhibitor molecules on CS surface is a spontaneous process [29-31].

### 3.4 Surface Morphology analysis

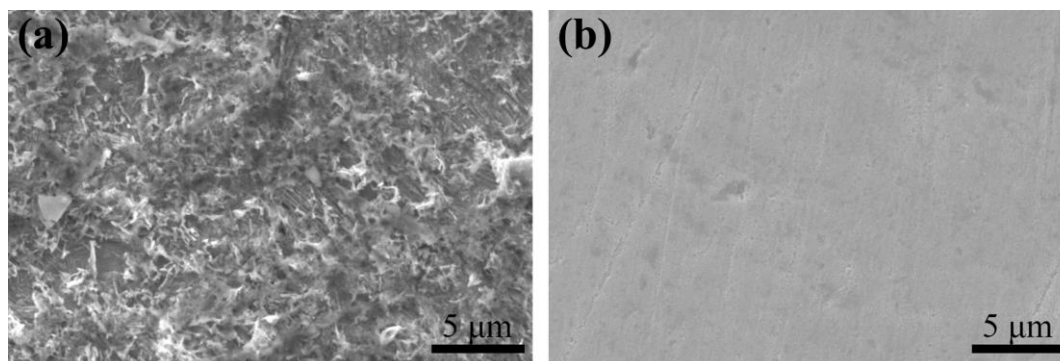


**Figure 7.** SEM images of CS after immersion in 0.5 M  $\text{H}_2\text{SO}_4$  (a) without inhibitor and (b) with 300mg/L of flubendazole

In order to give further evidence to the corrosion protection performance of flubendazole, surface morphologies of the CS in 0.5 M  $\text{H}_2\text{SO}_4$  without inhibitor and with 300 mg/L of flubendazole were recorded and displayed in Figure 7. As Fig. 7a shows, in comparison with the image as shown in Fig. 7b, without addition of the corrosion inhibitor, the roughness of metal surface is larger, and more corrosion pits appear on the surface of the sample after corrosion. After soaking of the sample in the solution with the corrosion inhibitor, the surface of the metal sample is relatively smooth and the overall structure is more uniform, the metal was protected well by flubendazole.

### 3.5 Theoretical calculation results

The frontier orbital of the inhibitor molecule can be used to evaluate the adsorption capacity of corrosion inhibitor on metal surface[32-34]. The distribution of the highest occupied molecular orbital (HOMO, Fig.8b) and lowest unoccupied molecular orbital (LUMO, Fig.8c) shows that the benzene ring, hydroxyl group and aromatic ring attached to benzene ring are major potential adsorption sites. The energy of the HOMO is  $-5.31 \text{ eV}$  while the energy of the LUMO is  $-2.35 \text{ eV}$ , and the dipole moment of the molecule is 6.72D. These values can give insights into the reaction reactivity of organic corrosion inhibitor [35, 36].

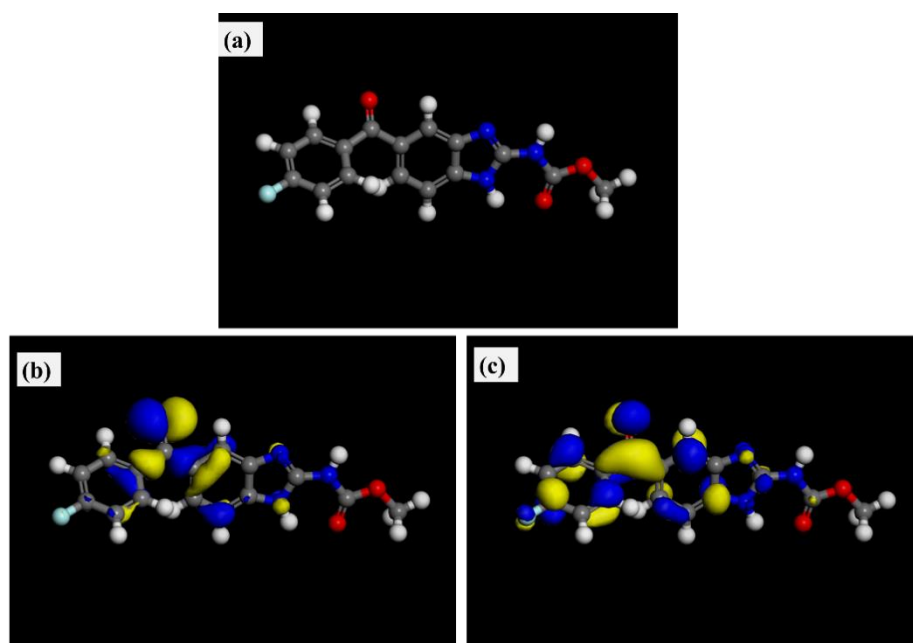


**Figure 8.** (a) Optimized structure, (b) HOMO and (c) LUMO of flubendazole

#### 4. CONCLUSION

The corrosion inhibition performance of flubendazole toward the corrosion of CS in 0.5 M H<sub>2</sub>SO<sub>4</sub> was studied, the main conclusions are as follows:

- (1) flubendazole adsorb on CS surface mainly through benzene ring, hydroxyl group and aromatic ring attached to benzene ring.
- (2) The adsorption of flubendazole on CS surface follows Langmuir isotherm.
- (3) The corrosion inhibition efficiency values of flubendazole increases with the increasing of the inhibitor concentration, and the maximum inhibition efficiency value is 93%.

#### References

1. M.B.R. Marija B. Petrović, Ana T. Simonović, Snežana M. Milić, Milan M. Antonijević, *Int. J. Electrochem. Sci.*, 7 (2012) 9043-9057.
2. Z. Chen, Z. Liu, K. He, G. Han, Y. Lv, J. Han, X. Wei, *Int. J. Electrochem. Sci.*, 16 (2021) 210559.
3. H. Li, S. Zhang, B. Tan, Y. Qiang, W. Li, S. Chen, L. Guo, *J. Mol. Liq.*, 305 (2020) 112789.
4. H. Li, Y. Qiang, W. Zhao, S. Zhang, *Corros. Sci.*, 191 (2021) 109715.
5. M.M.A. Marija B. Petrović Mihajlović, *Int. J. Electrochem. Sci.*, 10 (2015) 1027-1053.
6. Y. Qiang, S. Xu, L. Guo, N. Chen, Ime B. Obot, *Int. J. Electrochem. Sci.*, 11 (2016) 3147-3163.
7. M. Kasaeian, E. Ghasemi, B. Ramezanzadeh, M. Mahdavian, G. Bahlakeh, *Appl. Surf. Sci.*, 462 (2018) 963-979.
8. M. Ramezanzadeh, G. Bahlakeh, Z. Sanaei, B. Ramezanzadeh, *J. Mol. Liq.*, 272 (2018) 120-136.
9. Y. Qiang, L. Guo, S. Zhang, W. Li, S. Yu, J. Tan, *Sci. Rep.*, 6 (2016) 33305.
10. Y. Qiang, S. Zhang, S. Xu, W. Li, *J. Colloid. Interf. Sci.*, 472 (2016) 52-59.
11. L.O. Olasunkanmi, M.E. Mashuga, E.E. Ebenso, *Surf. Interfaces*, 12 (2018) 8-19.
12. W. Luo, W. Li, J. Tan, J. Liu, B. Tan, X. Zuo, Z. Wang, X. Zhang, *J. Mol. Liq.*, 314 (2020).
13. M.E. Mashuga, L.O. Olasunkanmi, C. Verma, E.-S.M. Sherif, E.E. Ebenso, *J. Mol. Liq.*, 305

(2020).

14. C. Li, Z. Sun, Mi. Kang, Z. Yan, Z. Tan, Q. Li, *Int. J. Electrochem. Sci.*, 16 (2021) 211034.
15. K.F. Khaled, *Electrochim. Acta.*, 54 (2009) 4345-4352.
16. D.-Q. Zhang, Q.-R. Cai, X.-M. He, L.-X. Gao, G.S. Kim, *Corros. Sci.*, 51 (2009) 2349-2354.
17. M.A. Amin, K.F. Khaled, *Corros. Sci.*, 52 (2010) 1194-1204.
18. K.F. Khaled, *Corros. Sci.*, 52 (2010) 3225-3234.
19. Y. Qiang, S. Zhang, L. Guo, X. Zheng, B. Xiang, S. Chen, *Corros. Sci.*, 119 (2017) 68-78.
20. Y. Qiang, S. Zhang, S. Yan, X. Zou, S. Chen, *Corros. Sci.*, 126 (2017) 295-304.
21. Y. Qiang, S. Fu, S. Zhang, S. Chen, X. Zou, *Corros. Sci.*, 140 (2018) 111-121.
22. H. Li, S. Zhang, Y. Qiang, *J. Mol. Liq.*, 321 (2021) 114450.
23. X. Zuo, W. Li, W. Luo, X. Zhang, Y. Qiang, J. Zhang, H. Li, B. Tan, *J. Mol. Liq.*, 321 (2021) 114914.
24. A. Döner, A.O. Yüce, G. Kardaş, *Ind. Eng. Chem. Res.*, 52 (2013) 9709-9718.
25. Sudheer, M.A. Quraishi, *Corros. Sci.*, 70 (2013) 161-169.
26. A. Zarrouk, B. Hammouti, A. Dafali, F. Bentiss, *Ind. Eng. Chem. Res.*, 52 (2013) 2560-2568.
27. Y. Qiang, S. Zhang, L. Wang, *Appl. Surf. Sci.*, 492 (2019) 228-238.
28. Y. Qiang, S. Zhang, H. Zhao, B. Tan, L. Wang, *Corros. Sci.*, 161 (2019) 108193.
29. A. Fiala, A. Chibani, A. Darchen, A. Boulkamh, K. Djebbar, *Appl. Surf. Sci.*, 253 (2007) 9347-9356.
30. K.M. Ismail, *Electrochim. Acta.*, 52 (2007) 7811-7819.
31. K.F. Khaled, *Appl. Surf. Sci.*, 255 (2008) 1811-1818.
32. Y. Qiang, H. Li, X. Lan, *J. Mater. Sci. Technol.*, 52 (2020) 63-71.
33. Y. Qiang, L. Guo, H. Li, X. Lan, *Chem. Eng. J.*, 406 (2021) 126863.
34. P. Han, C. Chen, W. Li, H. Yu, Y. Xu, L. Ma, Y. Zheng, *J. Colloid. Interf. Sci.*, 516 (2018) 398-406.
35. S. Pareek, D. Jain, S. Hussain, A. Biswas, R. Shrivastava, S.K. Parida, H.K. Kisan, H. Lgaz, I.-M. Chung, D. Behera, *Chem. Eng. J.*, 358 (2019) 725-742.
36. S. Ralkhal, T. Shahrabi, B. Ramezanzadeh, G. Bahlakeh, *Appl. Surf. Sci.*, 464 (2019) 178-194.